Biochemistry and Biophysics Reports 41 (2025) 101914

Contents lists available at ScienceDirect

Biochemistry and Biophysics Reports

journal homepage: www.elsevier.com/locate/bbrep

Human citrate synthase kinetic simulation to fit rapid, direct, and thiol probe coupled kinetic data

Noah Shackelford, Zach Zavodny, Samantha Schindler, Nathan Fancher, Allen A. Thomas, Michael A. Moxley *

Department of Chemistry, University of Nebraska at Kearney, USA

ARTICLE INFO

Keywords:
Enzyme kinetics
Global fitting
Kinetic simulation
Thiol probe
Citrate synthase

ABSTRACT

Human citrate synthase (hCS) was kinetically characterized through full progress curve kinetic modelling using kinetic simulation, global fitting of the direct AcCoA to CoA transition, and a coupled thiol probe reaction to better determine the kinetics with low substrate concentration. Our analysis provides one of the most rigorous kinetic analyses of any citrate synthase ruling out the need to invoke complex cooperative mechanisms to explain progress curve data. Furthermore, we collected and modeled stopped-flow pH-dependent kinetic data with CoA and popular thiol probes such as Ellman's reagent (DTNB) and 4,4′-Dithiodipyridine (DPS), providing the opportunity for detailed kinetic simulations using these thiol probes with CoA producing enzymes. Global fitting suggests that the DPS/CoA bimolecular rate constant increased 100-fold via protonation of the pyridine ring (pKa = 5.2), quantifying its kinetic advantage relative to DTNB. To explore the kinetic effects of polar substituents on the pyridine ring, we synthesized three different DPS analogs by adding either an alcohol, amine, or carboxylic acid moiety to the pyridine ring. Of these, the alcohol group provided the most similar kinetic characteristics to DPS but greatly increases thiol probe polarity offering an alternative to DPS.

1. Introduction

Citrate synthase (CS) catalyzes the aldol condensation of oxaloacetate and acetyl-CoA forming citrate and CoA in the first step of the tricarboxylic acid (TCA) cycle. CS activity is used as a metric for mitochondrial function [1], a regulator of TCA cycle flux [2], and its dysfunction is associated with metabolic disease [3].

Here we provide one of the most kinetically rigorous analyses of any CS by globally fitting a large collection of stopped-flow progress curves in the absence and presence of initially added products and natural nucleotide inhibitors AMP, ADP, and ATP. Our analysis of the CS stopped-flow progress curve data utilizes kinetic simulation to avoid simplifying steady-state and equilibrium assumptions [4]. Our analysis thus provides rate constants, which were used to calculate steady-state constants, including rigorously determined confidence intervals for these parameters [5,6]. We found that our data and modeling are consistent with an ordered bi bi mechanism, which might be the consensus mechanism for CS but has been challenged by some prominent enzymologists [7–11]. For example, mammalian CS have been reported to follow a bi bi ordered ternary mechanism [7,8], but hysteresis [9], cooperativity [10,11], and a rapid-equilibrium random-order ternary mechanism [11–13] have been proposed.

Importantly, we followed the CS catalyzed transition of AcCoA to CoA spectra directly, in the UV [6] rather than coupling the reaction to a thiol probe, to gain a more accurate kinetic signal. For example, CS kinetic data is most often followed by coupling the reaction using a thiol reactive probe such as DTNB (5,5′-dithiobis (2-nitrobenzoic acid)), also known as Ellman's reagent [11,13–15], to react with CoA. Since the reaction of DTNB with CoA is concentration and pH dependent [16,17], its addition complicates analysis of the kinetic data. Despite this, we have been unable to find an enzyme kinetic analysis that accounts for this typical coupling step.

Even though following the AcCoA to CoA transition without a coupling reaction is ideal, the absorbance difference in the UV is relatively minor making the reaction difficult to follow at low concentrations. Therefore, in the low concentration regime (<5 μM substrates) use of another chromophore can be beneficial, if correctly accounted for.

To more accurately account for the coupled CoA to thiol probe reaction, we collected and modeled pH-dependent stopped-flow progress curves with CoA and DTNB, and 4,4′-dithiodipyridine (DPS), another

* Corresponding author.
E-mail address: moxleyma@unk.edu (M.A. Moxley).

https://doi.org/10.1016/j.bbrep.2025.101914
Received 4 July 2024; Received in revised form 31 December 2024; Accepted 2 January 2025

popular thiol probe [18]. Global fitting of the CoA/DPS reaction progress curves required an additional proton binding step aligning with the pKa of the pyridine ring (pKa = 5.2), where proton binding increases the bimolecular rate constant by 100-fold.

To explore modifications of the pyridine ring on the kinetic performance of DPS with CoA, we synthesized three simple DPS analogs adding the following substituents: CH_2OH, $–CH_2NH_2$, and –COOH. We found that all modifications decreased the kinetic performance of DPS with CoA to some degree with the alcohol group having the least effect. However, increasing DPS polarity could decrease unwanted protein reactions, by avoiding non-polar protein environments to deter reaction with buried cysteine residues [19–21]. Thus, a more polar DPS analog, such as DPS- CH_2OH, not only increases water solubility but also provides an alternative probe to help avoid enzymatic inactivation.

2. Material and methods

2.1. Materials and reagents

Chemicals were purchased from Sigma-Aldrich and Fisher scientific, except CoA and acetyl-CoA were purchased from COALA biosciences (Austin, TX).

2.2. Human citrate synthase purification

Purified human citrate synthase was purchased through a customized protein purification project commissioned through Genscript (Piscataway, NJ). The wildtype human CS amino acid sequence was obtained from Uniprot ID: O75390 and used to generate the wildtype CS gene without the mitochondrial localization sequence. The protein was expressed using the pET30a expression vector with a N-term 6X histag. The plasmid was expressed in BL21 Star (DE3) cells and induced with 0.4 mM IPTG. Protein was purified with Ni-NTA chromatography and analyzed using SDS-PAGE, Western blot, and mass spectrometry. Protein concentration was determined by the Bradford protein assay with a final storage buffer of 50 mM Tris-HCl, 500 mM NaCl, 10 % glycerol at pH 8. Protein was stored at −80 °C.

2.3. Human citrate synthase stopped-flow assays and global fitting

All kinetic assays were performed at ambient temperature in 50 mM Tris at a pH of 7.8 and 0.25 μM CS with 0.22 μm filtered solutions. Kinetic absorption assays were performed on a KinTek SF-300X stopped-flow mixing device utilizing a deuterium lamp and followed using a multiwavelength CCD array detector. The CS reaction was followed by observing the absorbance change at 232 nm between acetyl-CoA and CoA, which has a molar extinction difference of approximately 2 mM^{-1} cm^{-1} [6]. Averaged kinetic data (at 232 nm) were then imported into KinTek Global Kinetic Explorer software (Austin, TX) and globally fitted to an ordered bi bi mechanism using non-linear least squares and numerical integration [4]. The CS reaction was also followed by adding DPS (4,4′-dithiodipyridine), 1.5 mM after mixing, where progress curves were fitted at 325 nm. All parameter sets that produced an error ratio ($error_{best\text{-}fit}/error_i$) threshold value within 0.833 of the best-fit value were used to determine upper and lower parameter bounds [5]. All kinetic figures were generated using MATLAB R2024a software.

2.4. DTNB/CoA, DPS/CoA, and DPS-x analog/CoA stopped-flow kinetics

DTNB (5,5′-dithiobis-(2-nitrobenzoic acid)) and CoA were rapidly mixed on a KinTek SF-300X stopped-flow mixing device utilizing a deuterium lamp and followed using a multiwavelength CCD array detector using a mixed buffering system at pH 6.5, 7.0, 7.5, 8.0, and 8.5. The mixed pH buffering system consisted of 50 mM HEPES, Tris, and histidine. Final concentrations of DTNB were 0.25, 0.5, 1.0 and 2.5 mM, with CoA at 0.125 mM after mixing. Single wavelength kinetic progress curves at 412 nm were then extracted from the multiwavelength data and globally fitted to the kinetic mechanism shown in Scheme 2A using KinTek Global Kinetic Explorer software. All kinetic figures were generated using MATLAB R2024a software.

DPS (4,4′-dithiodipyridine) and CoA were rapidly mixed in the same way as DTNB at pH 6.0, 6.5, 7.0, 7.5, and 8.0 using the same mixed buffering system as DTNB described above. These experiments were conducted by varying DPS concentrations at each pH, which were 0.25, 0.50, 1.0 and 1.5 mM with a fixed concentration of CoA at 0.10 mM, all after mixing. Single wavelength kinetic progress curves at 325 nm were then extracted from the multiwavelength data and globally fitted to the kinetic mechanism shown in Scheme 2B using KinTek Global Kinetic Explorer software. All DPS analog stopped-flow data collection and modeling were handled in the same way as DTNB.

2.5. Uncoupled/coupled hCS simulation comparison

Determined kinetic mechanisms and rate constants for hCS, DTNB/CoA, and DPS/CoA were used to conduct three separate simulations. All simulations were conducted with 0.25 μM hCS, 10 μM AcCoA, and 20 μM oxaloacetate for 1.25 s. The uncoupled reaction was simulated based on the signal of the molar absorptivity of the AcCoA/CoA spectral change. The DTNB coupled reaction signal was simulated using the fitted molar absorptivity of DTNB at 412 nm with 2.5 mM DTNB. The DPS coupled reaction used the fitted molar absorptivity of DPS as a signal at 325 nm with 1.5 mM DPS. Simulations were performed with KinTek Global Kinetic Explorer software. The final kinetic simulation figure was generated using MATLAB R2024a software.

2.6. Organic synthesis of DPS analogs

Thiol probes **DPS-X** ($\mathbf{X_a}$ = $–CH_2OH$, $\mathbf{X_b}$ = $–CH_2NH_2$, $\mathbf{X_c}$ = $–CO_2H$) were synthesized according to Scheme S1, in the supporting information where procedures are provided. As an example, for synthesis of the benzyl amine-containing disulfide ($\mathbf{X_b}$ = $–CH_2NH_2$), the primary amine of chloropyridine **1** was first protected using a Boc group. Displacement of **2**'s chlorine using sodium hydrosulfide gave thiopyridine analogs **3**. Oxidation of **3** using (diacetoxy)iodobenzene gave disulfides **DPS-X**, which were all purified by flash chromatography or recrystallization. Deprotection of the Boc amine for **DPS-$\mathbf{X_b}$'** ($\mathbf{X_b}$' = $–CH_2NHBoc$) using HCl gave desired **DPS-$\mathbf{X_b}$**. Disulfides were characterized by ^1H NMR and LC-MS.

3. Results and discussion

Mammalian CS have been reported to follow a bi bi ordered ternary mechanism [7,8], but hysteresis [9], cooperativity [10,11], and a rapid-equilibrium random-order ternary mechanism [11–13] have been proposed. Subsequent analysis of classic data sets from bovine heart, rat kidney and liver CS showed that many of these data could be best-fit to an ordered bi bi mechanism by globally fitting initial velocity data across several independent data sets [22].

Most published CS kinetic data sets are composed of initial velocity data often analyzed by double reciprocal plots [11,13,23]. Although the primary kinetic data, in progress curve data [6] has been shown in a few studies, it is not usually analyzed by the more modern approach of kinetic simulation [6,24], which models the primary data using less assumptions. To our knowledge, no large collection of CS kinetic data, from any organism, has been analyzed by the combination of kinetic simulation and global fitting. Therefore, our first objective was to accurately characterize the enzyme kinetics of human citrate synthase (hCS) by collecting full progress curve data and global fitting of the data with a model provided by kinetic simulation, including a rigorous confidence interval search of kinetic parameters.

Full progress curve data was collected by following the recombinant

hCS reaction in the forward direction using a stopped-flow mixer and CCD array multiwavelength detector (Fig. 1A). The hCS reaction was monitored while varying substrate concentration (Fig. 1B–E). For instance, hCS was separated from both substrates prior to stopped-flow mixing while varying the concentration of one substrate (Fig. 1B and D). Alternatively, hCS was pre-mixed with one of the substrates (oxaloacetate, Fig. 1C and AcCoA Fig. 1E) before mixing with the other substrate to determine effects of pre-mixing on the kinetics. Our variation in mixing strategy was implemented due to the observation that pre-mixing of AcCoA greatly inhibited a previously studied enzyme in carnitine acetyltransferase kinetics [6]. All progress curves were well fitted to an ordered bi bi kinetic mechanism (Scheme 1), with an added step for nucleotide inhibition characterized below. The data fitted in Fig. 1 is part of a global fit including data discussed below in Figs. 2 and 5.

Due to a report of detected reverse CS activity using a coupled enzyme system [11], we tried to monitor hCS activity in the reverse direction (Fig. 1F) using the non-coupled detection method and found that the change in absorbance is below the limit of detection. This result is consistent with an estimated equilibrium constant for the overall reaction at pH 7.8 being 1.2×10^7 [25].

To help determine the hCS kinetic mechanism, we collected product inhibition data with citrate and CoA. Notably, product inhibition with CoA cannot be carried out using the typical strategy of coupling the reaction with DTNB [11,13–15], since it would react with CoA. We found that along with all other data, product inhibition data were well fitted to an ordered bi bi mechanism (Fig. 2A and B).

By following the reaction using the AcCoA to CoA transition (Fig. 1) we found that the change in absorbance for substrates 5 μM and below was very minor. Therefore, we were interested in using a coupling reaction to better resolve the signal. Although it would be ideal to avoid a coupling reagent, explicitly accounting for the coupling reaction in the kinetic modeling while globally fitting both uncoupled and coupled data together can more accurately determine kinetic constants.

To this end, we explored two popular thiol probes, 4,4′-dithiodipyridine (DPS) [26] and Ellman's reagent (DTNB) [18], to determine which probe has better kinetics upon reaction with CoA. To accurately account for the kinetics of the reaction of DTNB with CoA, we collected pH and concentration dependent data with DTNB and CoA on the stopped-flow and modeled the data using global fitting (Fig. 3) based on the kinetic model shown in Scheme 2A. This model accounts for the CoA pK_a of 9 [27] and the second order reaction between CoA and DTNB (Scheme 2A). The fitted rate constant for this reaction can be found in Table S1.

When collecting data between DPS (Fig. 4) and CoA, we found an interesting difference between DTNB and DPS kinetics with CoA. To fit the DPS data, an extra protonation step is required in the kinetic mechanism (Scheme 2B), with a pK_a of 5.2 consistent with that on the pyridine ring. This step accounts for a faster reaction between DPS/CoA at lower pH compared to DTNB [28]. The pH-dependent kinetic difference between DTNB and DPS has been discussed elsewhere [28,29], but it has not been kinetically characterized by global fitting. Altogether the DPS/CoA two-step bimolecular rate constants were greater than the single step kinetic constant required to fit the DTNB/CoA kinetic data, with the protonated DPS species (DPSH+) rate constant being 100-fold greater than with DTNB (Scheme 2B and Table S1).

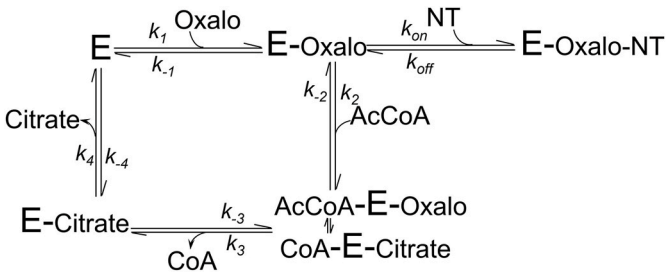

Scheme 1. Bi bi ordered ternary mechanism of citrate synthase, with the addition of a dead-end step for nucleotide (NT) inhibition. E denotes the enzyme.

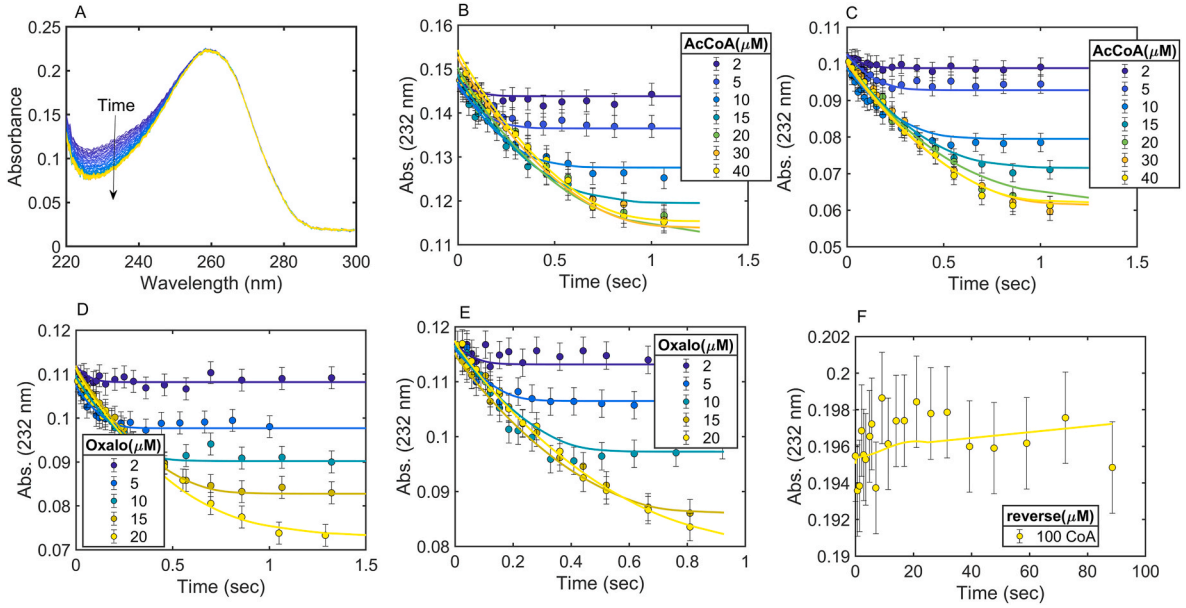

Fig. 1. hCS stopped-flow progress curves following AcCoA to CoA transition and globally fitted to an ordered bi-bi kinetic mechanism. A) Example of multiwavelength time-dependent CCD array scan of AcCoA transition to CoA by hCS. **B)** Fitted progress curves varying AcCoA and 20 μM oxaloacetate after mixing. **C)** Fitted progress curves varying AcCoA with hCS pre-mixed with oxaloacetate (20 μM after mixing). **D)** Fitted progress curves varying oxaloacetate with 20 μM AcCoA after mixing. **E)** Fitted progress curves varying oxaloacetate with hCS pre-mixed with 20 μM AcCoA after mixing. **F)** hCS reverse progress curve conditions of 100 μM CoA and 2 mM citrate. In B though F, data is shown as filled circles with line representing model prediction with matching color. Error bars represent standard deviations of the data. Starting absorbances were normalized to the highest absorbance to better observe all progress curves in a single figure panel. Global fitting also includes data in Fig. 2 and 5.

A

DTNB Kinetic Model

$$CoA\text{-}SH \overset{pKa = 9}{\rightleftharpoons} CoA\text{-}S^- + H^+$$

$$CoA\text{-}S^- + DTNB \xrightarrow{k_1} \text{Mixed disulfide} + TNB$$

B

DPS-x Kinetic Model

$$CoA\text{-}SH \overset{pKa = 9}{\rightleftharpoons} CoA\text{-}S^- + H^+$$

$$DPSH^+\text{-}x \overset{pKa = 5.2}{\rightleftharpoons} DPS\text{-}x + H^+$$

$$CoA\text{-}S^- + DPS\text{-}x \xrightarrow{k_1} \text{Mixed disulfide} + \text{thiopyridine}$$

$$CoA\text{-}S^- + DPSH^+\text{-}x \xrightarrow{k_2} \text{Mixed disulfide} + \text{thiopyridine}$$

Scheme 2. DTNB and DPS-x kinetic models. A) One step kinetic model of DTNB reacting with CoA, with CoA proton binding/dissociation equilibrium step. **B)** Two step kinetic model of DPS-x ($\mathbf{X_a}$ = $-CH_2OH$, $\mathbf{X_b}$ = $-CH_2NH_2$, $\mathbf{X_c}$ = $-CO_2H$) reacting with CoA, with CoA and DPS-x proton binding/dissociation equilibrium step.

After determining improved kinetics with DPS/CoA relative to DTNB, we chose to use DPS as a CoA probe for the hCS reaction. To theoretically account for the DPS/CoA reaction, we used the DPS/CoA fitted model (Scheme 2B) and rate constants (Table S1) to accurately account for the DPS/CoA coupled reaction at lower AcCoA and oxaloacetate concentrations to improve the signal (Fig. 5A and B). CS is inhibited by nucleotides such as ATP, ADP, and AMP [30], which are likely important for biochemical regulation of CS. Therefore, we generated these data sets to include inhibition by AMP (Fig. 5C), ADP (Fig. 5D), and ATP (Fig. 5E) to create a more comprehensive data set for hCS kinetic modeling. Since each of these nucleotides absorb strongly in the AcCoA-to-CoA spectral region, following these reactions using the direct method is not feasible. Therefore, we used the DPS coupling method to collect data and corresponding kinetic modeling and global fitting to simulate the experiments. Each nucleotide inhibitor was included in the mechanism and simulated by competing for the AcCoA/CoA binding site, with oxaloacetate bound (Scheme 1).

All hCS data (Figs. 1, 2 and 5) were simultaneously fitted, or globally fitted, using non-linear least squares fitting to the numerically integrated solution of the ordered bi bi kinetic mechanism including nucleotide inhibition (Scheme 1). The global simulation also includes Scheme 2B kinetic steps when accounting for the DPS/CoA reaction using the rate constants found in Table S1. Fitting the data in this manner directly estimates rate constants (Table 1) that were then used to calculate steady-state constants (Table 2), as previously discussed for the bi bi kinetic mechanism [6].

To estimate rigorous confidence intervals for rate constants and then steady-state constants, we implemented a computation within KinTek Global Explorer software that systematically adjusts parameter values while calculating the error between the model prediction and the data. All parameter sets that produce an error ratio ($error_{best\text{-}fit}/error_i$) threshold value within 0.833 of the best-fit value were used to determine upper and lower parameter bounds (Table 1) [5]. As expected, rate constants (Table 1) are difficult to constrain relative to steady-state kinetic constants (Table 2) [4,5].

To compare methods of following CS, we simulated progress curves based on the determined rate constants (Fig. 6). Our simulation shows that DPS responds more quickly and accurately to the production of CoA relative to DTNB, while providing a better signal even at pH 7.8.

We looked to commercial sources to find DPS analogs to further improve DPS/CoA reactivity and DPS polarity but could only find analogs that would increase the likelihood of an unwanted reaction or would decrease polarity. Therefore, we synthesized a few simple DPS analogs by modifying the pyridine ring with the following substituents: CH_2OH, $-CH_2NH_2$, and –COOH (Scheme 3).

We found that the DPS-CH_2OH analog (Scheme 3) had the most similar kinetics at pH 7 (Fig. 7C) and 8 (Fig. 7F) to DPS, with a 15 % drop in apparent equilibrium. Therefore, we generated a full concentration and pH-dependent data set and modeled the data as with DPS (Fig. S1), and further confirmed that the DPS-CH_2OH analog gave similar rate constants to DPS (Fig. 8 and Table S1). The DPS-CH_2NH_2 analog demonstrated a much greater drop in apparent equilibrium (2.5-fold), which would severely limit its use at 325 nm (Figs. S2C and F); although a larger absorbance change is seen at about 290 nm (Fig. S2E). Given the apparent decrease in equilibrium and/or signal we decided not to pursue this probe further.

The DPS-COOH analog demonstrated similar kinetics at pH 8 (Fig. S3F) to DPS and somewhat attenuated kinetics at pH 7 (Fig. S3C). Notably, the absorbance maximum red shifted from 325 nm with DPS to 337 nm in DPS-COOH. We generated a concentration and pH-dependent

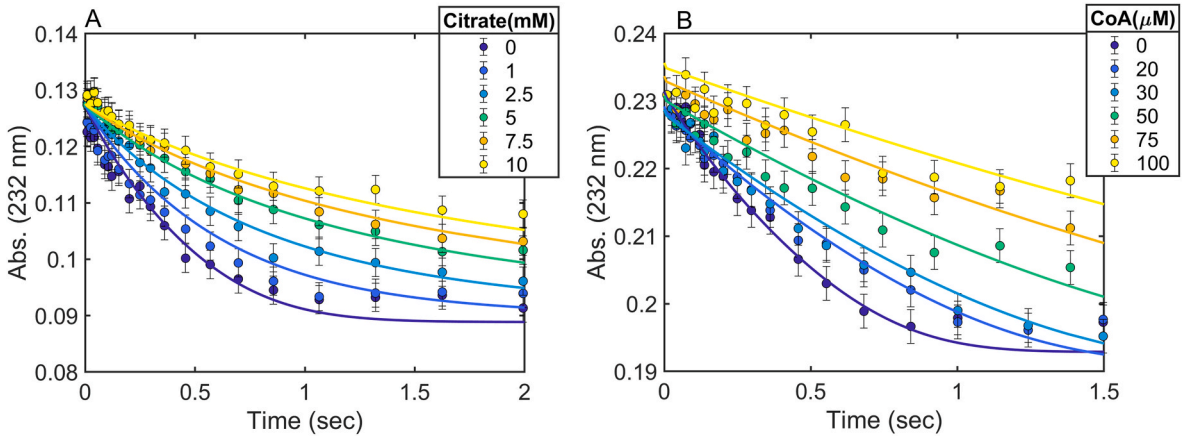

Fig. 2. hCS stopped-flow progress curves with added products following AcCoA to CoA transition globally fitted to an ordered bi-bi kinetic mechanism. A) Fitted progress curves of hCS with pre-mixed oxaloacetate mixed against AcCoA and varied Citrate. **B)** Fitted progress curves of hCS with pre-mixed oxaloacetate mixed against AcCoA and varied CoA. Data is shown as filled circles with line representing model prediction with matching color. Error bars represent standard deviations of the data. Starting absorbances were normalized to the highest absorbance to better observe all progress curves in a single figure panel. Global fitting also includes data in Fig. 1 and 5.

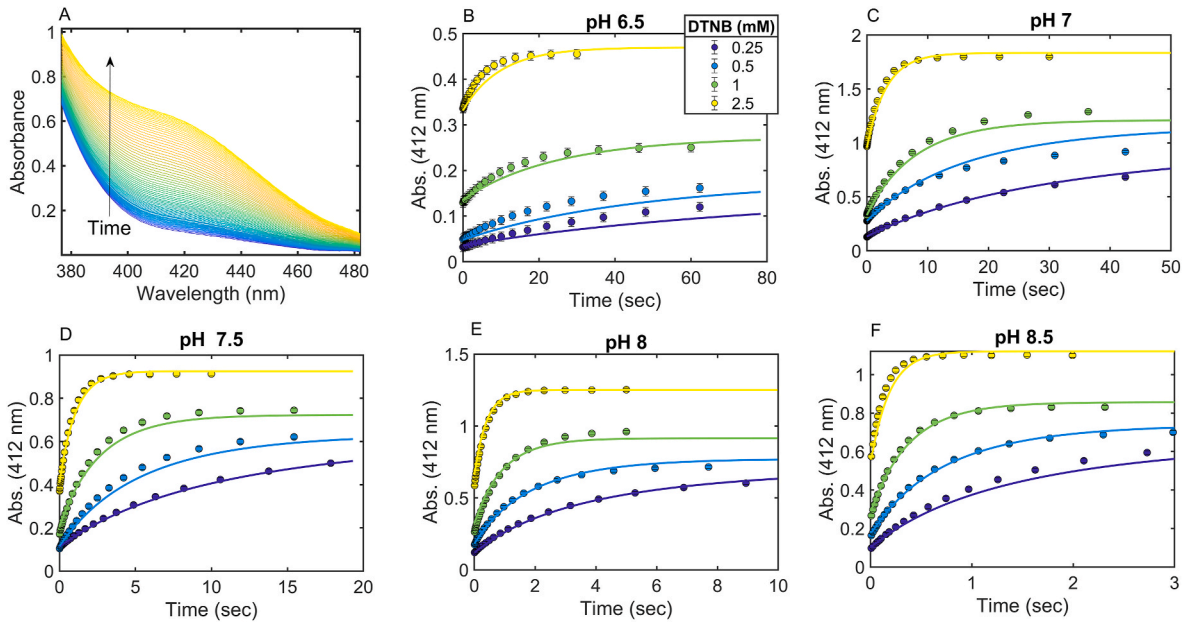

Fig. 3. Global fitting of DTNB concentration and pH-dependent stopped-flow progress curves with CoA. A) Example of multiwavelength time-dependent detection of DTNB and CoA reaction with CCD array dector at pH 8.5. **B–F)** Panels B through F show data (circles) with pH given in the title plotted against the predicted line with matching color from the global fitting of the kinetic model (Scheme 2A). All panels have varied amounts of DTNB as shown in the legend in panel B.

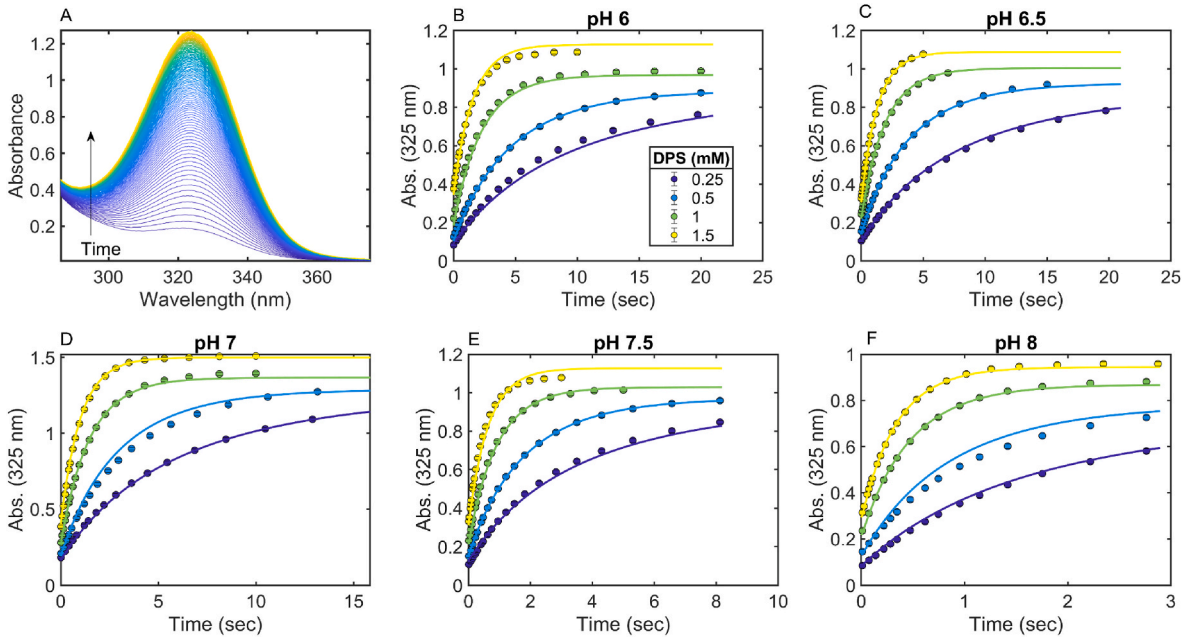

Fig. 4. Global fitting of DPS concentration and pH-dependent stopped-flow progress curves with CoA. A) Example of multiwavelength time-dependent detection of DPS and CoA reaction with CCD array dector at pH 7. **B–F)** Panels B through F show data (circles) with pH given in the title plotted against the predicted line with matching color from the global fitting of the kinetic model (Scheme 2B). All panels have varied amounts of DPS as shown in the legend in panel B.

data set to determine the full impact of the carboxylic acid (Fig. S4) and found that the carboxylic acid moiety reduced rate constants by about a factor of three overall (Fig. 8 and Table S1).

4. Conclusions

Here we applied modern kinetic simulation and global fitting methods to human citrate synthase (hCS) stopped-flow progress curves to provide a comprehensive and consistent data set, delivering one of the most rigorously determined models of this enzyme. Our progress curve data and modelling strategy supports the ordered bi bi mechanism for hCS rather than the need to invoke more complex cooperative [10,11] or hysteric [9] mechanisms that have been suggested in the past.

The majority of our hCS kinetic data was collected by following the direct UV spectral change between AcCoA and CoA [6], rather than coupling the reaction to a thiol probe such as DTNB or Ellman's reagent, which is the common strategy to follow CoA producing enzymatic reactions [11,13–15,31–41]. This strategy allowed for a more direct kinetic analysis of the hCS data, which provided the ability to monitor CoA inhibition and the reverse hCS reaction. However, we found that at

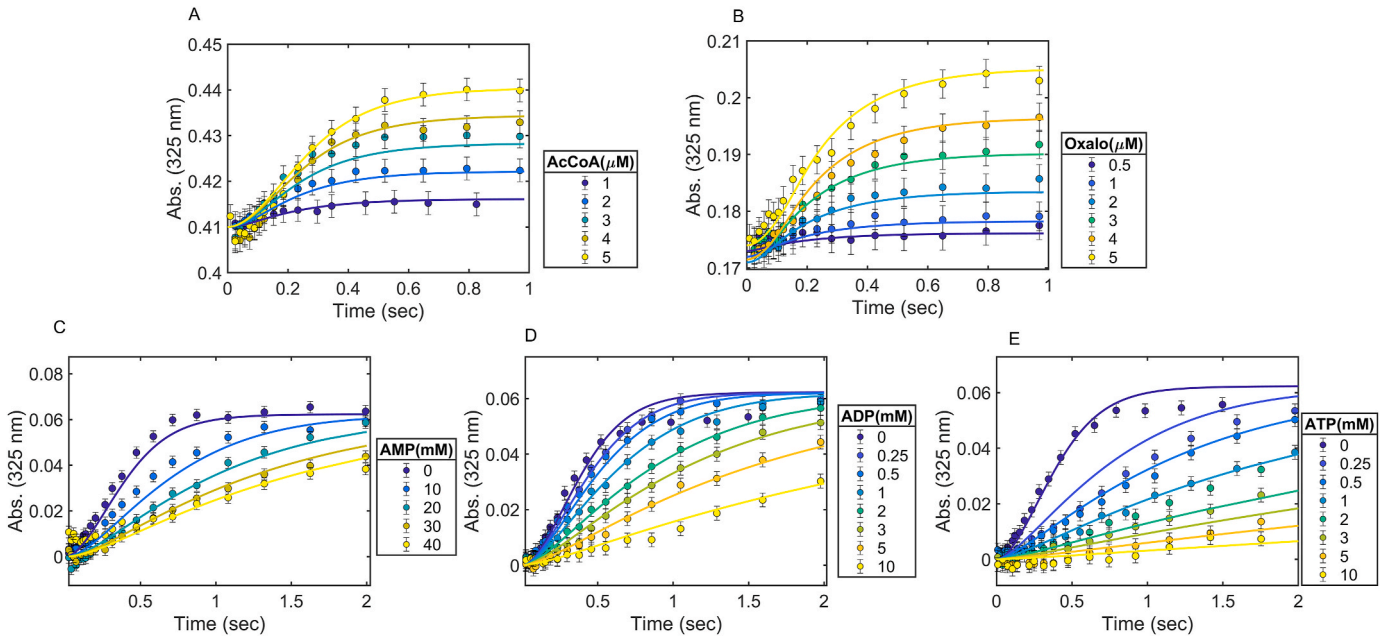

Fig. 5. hCS stopped-flow progress curves with nucleotide inhibition coupled with DPS and globally fitted to ordered bi bi kinetic mechanism. A) Fitted progress curves of hCS varying AcCoA with pre-mixed oxaloacetate followed at 325 nm with DPS. **B)** Fitted progress curves of hCS varying oxaloacetate with pre-mixed AcCoA and followed at 325 with DPS. **C)** Fitted progress curves of hCS with pre-mixed oxaloacetate against AcCoA and varied AMP followed at 325 nm with DPS. **D)** Fitted progress curves of hCS with pre-mixed oxaloacetate against AcCoA and varied ADP followed at 325 nm with DPS. **E)** Fitted progress curves of hCS with pre-mixed oxaloacetate against AcCoA and varied AMP followed at 325 nm with DPS. Data is shown as filled circles with line representing model prediction with matching color. Error bars are standard deviations of the data. Starting absorbances were normalized to the highest absorbance to better observe all progress curves in a single figure panel. Global fitting also includes data in Figs. 1 and 2. DPS reaction with CoA was modeled using Scheme 2B using rate constants found in Table S1.

Table 1
Human citrate synthase globally fitted rate constants from ordered bi-bi mechanism.

Rate constant	Best-fit	[a]Lower bound	[a]Upper bound
k_1 ($\mu M^{-1}s^{-1}$)	91.9	36.7	916
k_{-1} (s^{-1})	0.113	1.13×10^{-4}	1.13
k_2 ($\mu M^{-1}s^{-1}$)	161	33.7	1.61×10^{3}
k_{-2} (s^{-1})	1140	131	1.15×10^{3}
k_3 (s^{-1})	830	234	1.32×10^{4}
k_{-3} ($\mu M^{-1}s^{-1}$)	48	12.6	481
k_4 (s^{-1})	273	148	822
k_{-4} ($\mu M^{-1}s^{-1}$)	0.758	0.197	6.42

[a] Upper and lower bounds were calculated from the maximum and minimum calculated parameters within a 0.83 relative error threshold [5].

Table 2
[a]Calculated steady-state constants for the ordered bi-bi mechanism and inhibition constants.

Steady-state constant	Best-fit	[b]Lower bound	[b]Upper bound
$k_{cat}^{f}(s^{-1})$	225	138	578
$K_m^{Oxalo}(\mu M)$	2.51	0.19	15.3
$K_m^{AcCoA}(\mu M)$	4.24	1.08	9.42
$K_i^{AcCoA}(\mu M)$	8.55	1.39	37.8
$K_i^{CoA}(\mu M)$	22.3	6.17	60.3
$K_m^{Citrate}(\mu M)$	380	34.9	1.64×10^{3}
$K_i^{ATP}(mM)$	0.0449	0.0157	0.0841
$K_i^{ADP}(mM)$	0.301	0.101	0.536
$K_i^{AMP}(mM)$	2.16	0.910	4.59

[a] Steady-steady constants were calculated as previously described for the bi bi kinetic mechanism [6].

[b] Upper and lower bounds were calculated from the maximum and minimum calculated parameters within a 0.83 relative error threshold [5].

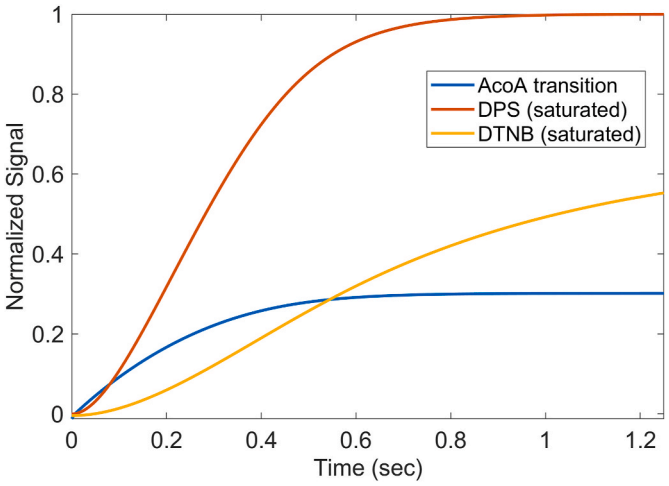

Fig. 6. Comparison of kinetic simulations of human citrate synthase activity followed by different methods. The human citrate synthase kinetic model was simulated and followed by either the AcCoA to CoA spectral transition (blue), DPS thiol probe in saturating conditions (red, 1.5 mM), or DTNB thiol probe in saturating conditions (gold, 2.5 mM). To better compare the signals, the simulated progress curves were normalized to zero.

substrate concentrations below 5 μM this strategy suffered from low signal. To circumvent this, we kinetically characterized the reaction between CoA and DTNB and another thiol probe, DPS [17–19,26,28,42,43]. By using stopped-flow and global fitting kinetic methods, we determined that the DPS/CoA rate constant improved at least 100-fold over DTNB at lower pH by incorporating an additional kinetic step accounting for protonation of the pyridine ring. We then merged the bi bi ordered kinetic mechanism of hCS with the DPS coupling mechanism to simulate hCS data with DPS at low substrate concentration, which also

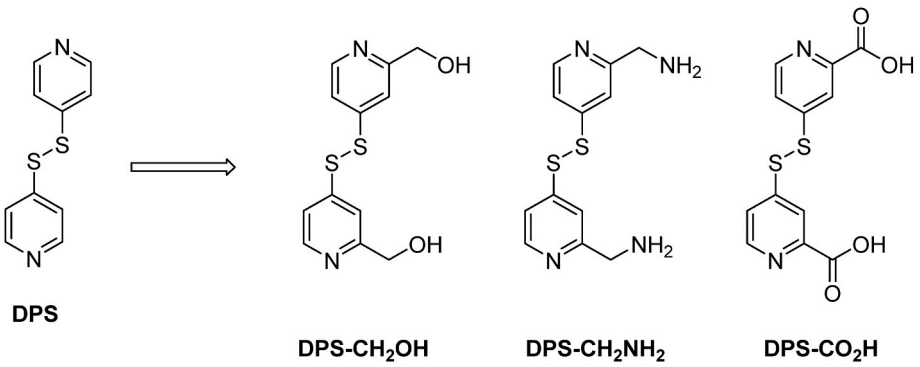

Scheme 3. 4,4′-Dithiodipyridine (DPS) analogs.

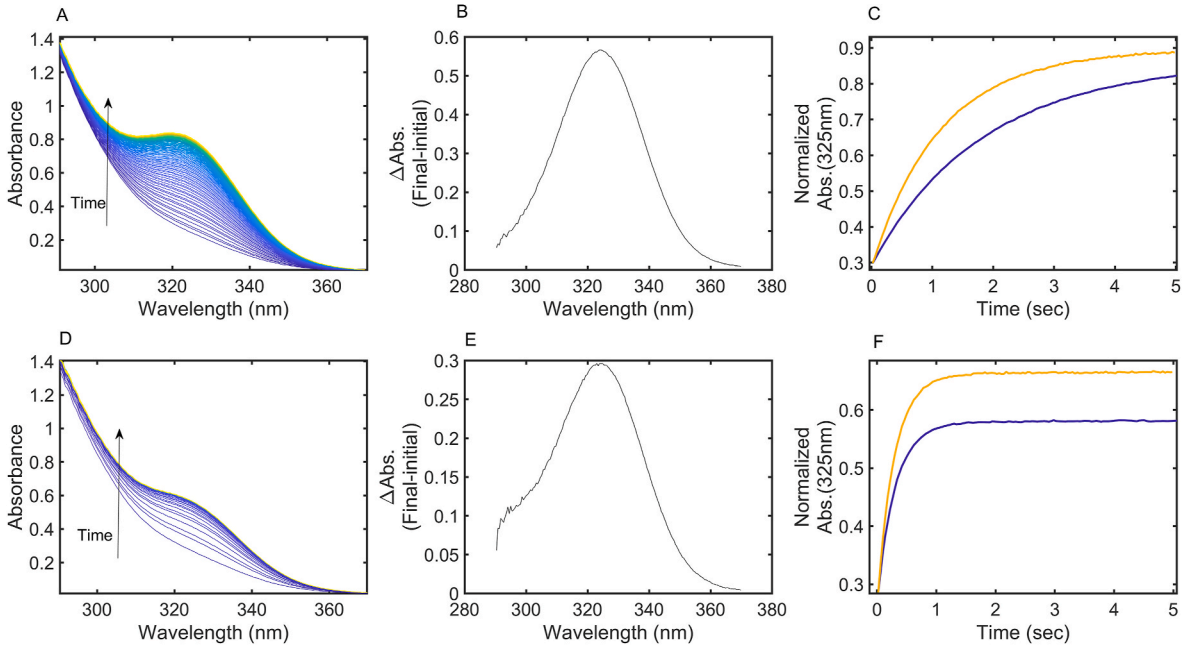

Fig. 7. DPS-CH_2-OH stopped-flow kinetics with DPS control. A) DPS–CH_2–OH rapidly mixed (1.5 mM after mixing) with CoA (0.1 mM after mixing) at pH 7, following UV–Vis spectra as a function of time. **B)** Difference spectra between first and last spectra from panel A. **C)** Single wavelength kinetic trace at 325 nm for both DPS (gold) and DPS–CH_2–OH (blue) at pH 7. **D)** DPS–CH_2–OH rapidly mixed (1.5 mM after mixing) with CoA (0.1 mM after mixing) at pH 8, following UV–Vis spectra as a function of time. **E)** Difference spectra from panel D. **F)** Single wavelength kinetic trace at 325 nm for both DPS (gold) and DPS–CH_2–OH (blue) at pH 8.

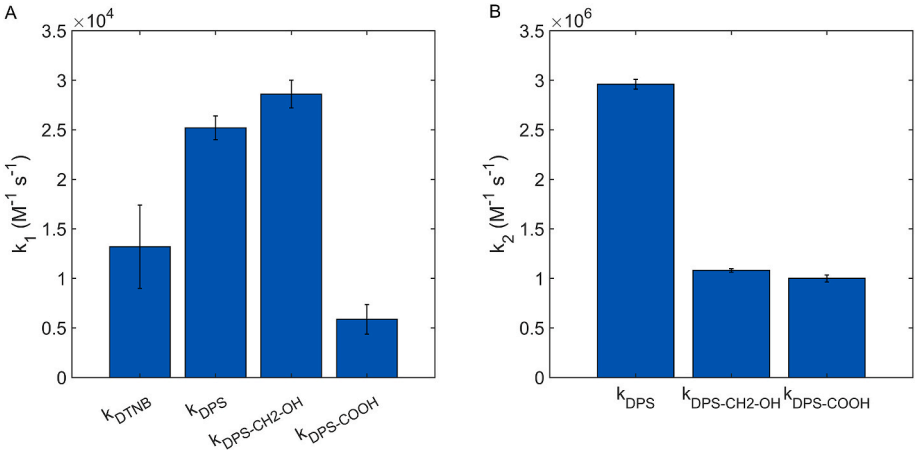

Fig. 8. Thiol probe/CoA reaction rate constants. A) The k_1 rate constant for respective thiol probe with CoA shown in Scheme A or B. **B)** The k_2 rate constant for respective thiol probe with CoA shown in Scheme B. Standard deviations are represented by error bars.

enabled nucleotide inhibition (K_i) estimation.

Like DTNB, DPS has also been used as a thiol probe for enzyme kinetic analysis [19,42,43], but to a much lesser degree probably due to its non-polar properties causing it to permeate enzymes and inactivate them [20,21]. Some have implemented site directed mutagenesis of the enzyme to avoid reaction of cysteine residues with DPS [19]. Analogs of DPS, with selectable characteristics such as increased polarity, or negative and positive charges could help to avoid unwanted probe reactions. To this end, we synthesized three simple DPS analogs with the following substituents: CH_2OH, $–CH_2NH_2$, and –COOH. Of these, we found that the DPS-CH_2OH and DPS-COOH analogs had the most similar kinetic characteristics to the original DPS and could serve as a more polar alternative to DPS to potentially decrease the possibility of adverse protein interactions due to a non-polar thiol probe.

CRediT authorship contribution statement

Noah Shackelford: Validation, Investigation. **Zach Zavodny:** Investigation. **Samantha Schindler:** Investigation. **Nathan Fancher:** Investigation. **Allen A. Thomas:** Writing – review & editing, Visualization, Methodology, Investigation, Data curation. **Michael A. Moxley:** Writing – review & editing, Writing – original draft, Visualization, Validation, Supervision, Resources, Project administration, Methodology, Investigation, Funding acquisition, Formal analysis, Data curation, Conceptualization.

Data availability

Data will be made available on request.

Funding

This work was financially supported by the National Institutes of Health grants 5P20GM103427 and 1R15GM152925-01.

Declaration of competing interest

The authors declare that they have no known competing financial interests or personal relationships that could have appeared to influence the work reported in this paper.

Appendix A. Supplementary data

Supplementary data to this article can be found online at https://doi.org/10.1016/j.bbrep.2025.101914.

References

[1] A. Vigelso, N.B. Andersen, F. Dela, The relationship between skeletal muscle mitochondrial citrate synthase activity and whole body oxygen uptake adaptations in response to exercise training, Int J Physiol Pathophysiol Pharmacol 6 (2014) 84–101.
[2] P.K. Arnold, L.W.S. Finley, Regulation and function of the mammalian tricarboxylic acid cycle, J. Biol. Chem. 299 (2023) 102838.
[3] I. Martinez-Reyes, N.S. Chandel, Mitochondrial TCA cycle metabolites control physiology and disease, Nat. Commun. 11 (2020) 102.
[4] K.A. Johnson, Z.B. Simpson, T. Blom, Global kinetic explorer: a new computer program for dynamic simulation and fitting of kinetic data, Anal. Biochem. 387 (2009) 20–29.
[5] K.A. Johnson, Z.B. Simpson, T. Blom, FitSpace explorer: an algorithm to evaluate multidimensional parameter space in fitting kinetic data, Anal. Biochem. 387 (2009) 30–41.
[6] M.J. Kratochvil, N.K. Balerud, S.J. Schindler, M.A. Moxley, Evidence of a preferred kinetic pathway in the carnitine acetyltransferase reaction, Arch. Biochem. Biophys. 691 (2020) 108507.
[7] C.J. Johansson, G. Pettersson, Kinetics of the inhibition of citrate synthase from pig heart by substrate analogues, Eur. J. Biochem. 46 (1974) 5–11.
[8] L.C. Kurz, T. Nakra, R. Stein, W. Plungkhen, M. Riley, F. Hsu, G.R. Drysdale, Effects of changes in three catalytic residues on the relative stabilities of some of the intermediates and transition states in the citrate synthase reaction, Biochemistry 37 (1998) 9724–9737.
[9] G. Lohlein-Werhahn, E. Bayer, B. Bauer, H. Eggerer, Hysteretic behaviour of citrate synthase. Alternating sites during the catalytic cycle, Eur. J. Biochem. 133 (1983) 665–672.
[10] L.C. Kurz, S. Shah, C. Frieden, T. Nakra, R.E. Stein, G.R. Drysdale, C.T. Evans, P. A. Srere, Catalytic strategy of citrate synthase: subunit interactions revealed as a consequence of a single amino acid change in the oxaloacetate binding site, Biochemistry 34 (1995) 13278–13288.
[11] Y. Matsuoka, P.A. Srere, Kinetic studies of citrate synthase from rat kidney and rat brain, J. Biol. Chem. 248 (1973) 8022–8030.
[12] D. Shepherd, P.B. Garland, The kinetic properties of citrate synthase from rat liver mitochondria, Biochem. J. 114 (1969) 597–610.
[13] C.J. Johansson, A. Mahlen, G. Petterson, Kinetic studies on citrate synthase from pig heart, Biochim. Biophys. Acta 309 (1973) 466–472.
[14] X.E. Wilcox, A. Ariola, J.R. Jackson, K.M. Slade, Overlap concentration and the effect of macromolecular crowding on citrate synthase activity, Biochemistry 59 (2020) 1737–1746.
[15] H.R. Ellis, Quantifying sulfur compounds with Ellman's reagent, Arch. Biochem. Biophys. (2022) 109174.
[16] G. Legler, 4,4'-Dinitrodiphenyldisulfides of different charge type as probes for the electrostatic environment of sulfhydryl groups, Biochim. Biophys. Acta 405 (1975) 136–143.
[17] C.K. Riener, G. Kada, H.J. Gruber, Quick measurement of protein sulfhydryls with Ellman's reagent and with 4,4'-dithiodipyridine, Anal. Bioanal. Chem. 373 (2002) 266–276.
[18] J.R. Winther, C. Thorpe, Quantification of thiols and disulfides, Biochim. Biophys. Acta 1840 (2014) 838–846.
[19] C.E. Quartararo, J.S. Blanchard, Kinetic and chemical mechanism of malate synthase from Mycobacterium tuberculosis, Biochemistry 50 (2011) 6879–6887.
[20] R. Svensson, R. Rinaldi, S. Swedmark, R. Morgenstern, Reactivity of cysteine-49 and its influence on the activation of microsomal glutathione transferase 1: evidence for subunit interaction, Biochemistry 39 (2000) 15144–15149.
[21] Q.K. Huynh, E.A. Gulve, T. Dian, Purification and characterization of glutamine: fructose 6-phosphate amidotransferase from rat liver, Arch. Biochem. Biophys. 379 (2000) 307–313.
[22] D.A. Beard, K.C. Vinnakota, F. Wu, Detailed enzyme kinetics in terms of biochemical species: study of citrate synthase, PLoS One 3 (2008) e1825.
[23] P.A. Srere, Y. Matsuoka, A. Mukherjee, Inhibition studies of rat citrate synthase, J. Biol. Chem. 248 (1973) 8031–8035.
[24] K.A. Johnson, Fitting enzyme kinetic data with KinTek global kinetic explorer, Methods Enzymol. 467 (2009) 601–626.
[25] A. Flamholz, E. Noor, A. Bar-Even, R. Milo, eQuilibrator–the biochemical thermodynamics calculator, Nucleic Acids Res. 40 (2012) D770–D775.
[26] I.O. Egwim, H.J. Gruber, Spectrophotometric measurement of mercaptans with 4,4'-dithiodipyridine, Anal. Biochem. 288 (2001) 188–194.
[27] D.A. Keire, J.M. Robert, D.L. Rabenstein, Microscopic protonation equilibria and solution conformations of coenzyme A and coenzyme A disulfides, J. Org. Chem. 57 (1992).
[28] R.L.W.C.E. Grimshaw, W.W. Cleland, Ring opening and closing rates for thiosugars, J. Am. Chem. Soc. 101 (1979).
[29] R.E. Hansen, H. Ostergaard, P. Norgaard, J.R. Winther, Quantification of protein thiols and dithiols in the picomolar range using sodium borohydride and 4,4'-dithiodipyridine, Anal. Biochem. 363 (2007) 77–82.
[30] N.O. Jangaard, J. Unkeless, D.E. Atkinson, The inhibition of citrate synthase by adenosine triphosphate, Biochim. Biophys. Acta 151 (1968) 225–235.
[31] G.L. Ellman, Tissue sulfhydryl groups, Arch. Biochem. Biophys. 82 (1959) 70–77.
[32] M.L. Sullivan, Near-real time determination of BAHD acyl-coenzyme A transferase reaction rates and kinetic parameters using Ellman's reagent, Methods Enzymol. 683 (2023) 19–39.
[33] T. Tuzimski, A. Petruczynik, M. Szultka-Mlynska, M. Sugajski, B. Buszewski, Isoquinoline alkaloid contents in macleaya cordata extracts and their acetylcholinesterase and butyrylcholinesterase inhibition, Molecules 27 (2022).
[34] F. Marchesani, E. Zangelmi, S. Bruno, S. Bettati, A. Peracchi, B. Campanini, A novel assay for phosphoserine phosphatase exploiting serine acetyltransferase as the coupling enzyme, Life (Basel) 11 (2021).
[35] A.R. Mukhametgalieva, I.V. Zueva, A.R. Aglyamova, S.V. Lushchekina, P. Masson, A new sensitive spectrofluorimetric method for measurement of activity and kinetic study of cholinesterases, Biochim Biophys Acta Proteins Proteom 1868 (2020) 140270.
[36] M.L. Sullivan, N.D. Bonawitz, Spectrophotometric determination of reaction rates and kinetic parameters of a BAHD acyltransferase using DTNB (5,5'-dithio-bis-[2-nitrobenzoic acid]), Plant Sci. 269 (2018) 148–152.
[37] C. Andreessen, N. Wolf, B. Cramer, H.U. Humpf, A. Steinbuchel, In vitro biosynthesis of 3-mercaptolactate by lactate dehydrogenases, Enzyme Microb Technol 108 (2018) 1–10.
[38] D. Andrew Skaff, H.M. Miziorko, A visible wavelength spectrophotometric assay suitable for high-throughput screening of 3-hydroxy-3-methylglutaryl-CoA synthase, Anal. Biochem. 396 (2010) 96–102.
[39] E.W. Brooke, S.G. Davies, A.W. Mulvaney, F. Pompeo, E. Sim, R.J. Vickers, An approach to identifying novel substrates of bacterial arylamine N-acetyltransferases, Bioorg. Med. Chem. 11 (2003) 1227–1234.
[40] K. Kume, T. Shimizu, Y. Seyama, Characterization of sn-glycerol 3-phosphate acyltransferase from Guinea pig harderian gland microsomes, J. Biochem. 101 (1987) 653–660.

[41] W. Zheng, K.A. Scheibner, A.K. Ho, P.A. Cole, Mechanistic studies on the alkyltransferase activity of serotonin N-acetyltransferase, Chem. Biol. 8 (2001) 379–389.
[42] J.W. Williams, D.B. Northrop, Kinetic mechanisms of gentamicin acetyltransferase I. Antibiotic-dependent shift from rapid to nonrapid equilibrium random mechanisms, J. Biol. Chem. 253 (1978) 5902–5907.
[43] K. Radika, D.B. Northrop, The kinetic mechanism of kanamycin acetyltransferase derived from the use of alternative antibiotics and coenzymes, J. Biol. Chem. 259 (1984) 12543–12546.